International Journal of Current Engineering and Technology ISSN 2277 - 4106

Available at http://inpressco.com/category/ijcet

Research Article

Structural, Electrical and Magnetic Studies of Gd $^{3+}$ doped Cobalt Ferrite Nanoparticles

Erum Pervaiz[a] and I.H.Gul[a*]

[a]Thermal Transport Laboratory (TTL), Department of Materials Engineering, School of Chemical and Materials Engineering (SCME), National University of Sciences and Technology (NUST), H-12 Islamabad., Pakistan.

Accepted 4 Nov.2012, Available online 1Dec. 2012, **Vol.2, No.4(Dec. 2012)**

Abstract

Gd^{3+} doped nanocrystalline Co-ferrites $CoGd_xFe_{2-x}O_4$ (x =0.0 to 0.1) has been prepared by sol-gel auto combustion technique. Structural and morphology studies were performed using X-ray diffraction (XRD), Fourier Transform Infrared Spectroscopy (FT-IR), Scanning Electron Microscopy (SEM) and Atomic Force Microscopy (AFM). Indexed XRD patterns confirm the formation of pure cubic spinel phase. Average crystallite sizes ranges from 16 nm to 25 nm ±2. Lattice constant (a) and crystallite size D (311) increases with increase in Gd^{3+} concentration due to large ionic radii (0.94nm) of Gd^{3+} replacing Fe^{3+} (0.64nm). FT-IR analysis shows the presence of two expected bands attributed to tetrahedral and octahedral metal oxygen vibrations. SEM images show the spherical morphology and uniform size distribution. Room temperature DC electrical resistivity decreases (~10^6) for x=0.025 then increases up to x=0.1 ~ (2.67x10^8) Ω-cm. Dielectric properties have been studied in the frequency range of 1 kHz to 5 MHz. Permittivity and tangent loss (tanδ) decreases with the substitution of Gd^{3+} in parent crystal structure and have values of 12.4 and 0.0160 at 5 MHz respectively. Complex impedance plots were further studied for complete contribution of grains and grain boundary resistances. Magnetic studies shows that magnetization (Ms) decreases with increase in Gd^{3+} concentration from 63 emu/gm to 27.26 emu/gm, thus the material is becoming low loss dielectric, highly resistive and soft magnetic due to Gd^{3+} doping.

Keywords: *Rare earth ions, XRD, W-H plots, Dielectric properties, AC conductivity, magneto crystalline anisotropy*

1. Introduction

Nano phase ferrites are a class of magnetic materials that have been the most attractive area of the research since the last 5 decades due to its remarkable applications in the high frequency and power devices especially for electromagnetic interference suppression (EMIS), phase shifters and circulators for mobile phones (R. Valenzuela *et al*., 2012). Spinel ferrites have many versatile electric and magnetic properties owing to its feasibility to make a huge number of solid solutions of different metal cations and a large compositional variability. As the crystal structure of spinel ferrite is cubic closed pack (fcc) with anions (O^{2-}) linked with two sub-lattices namely tetrahedral (A) and octahedral (B). Distribution of divalent and trivalent cations on the A and B sites imparts specific characteristics to a spinel structure (L. B. Tahar *et al.*, 2008). $CoFe_2O_4$ is a well known partially inverse spinel, ferromagnetic material with a high specific resistance, low losses in high frequency applications, high coercivity and a moderate saturation magnetization with positive magneto-crystalline anisotropy (M. A. Elkestawy *et a.l.*, 2010). These exceptional physical properties can be achieved by choosing the method of synthesis, doping of cation in the host crystal structure, size and morphology of the particles. Various methods has been adopted for the synthesis of cobalt ferrites which includes chemical co-precipitation (Y. I. Kim *et al.*, 2003), sol-gel (C. S. Kim *et al.*, 1999), hydrothermal (J. Peng *et al.*, 2011), microemulsion (V. Pillai *et al.*, 1996), solvothermal (W.

Cai *et al.*, 2007), reverse micelle (E. E. Sielo *et al.*, 2004), citrate precursor (M. M. Rashad *et al.*, 2008), and solid state reaction (K. S. Rao *et al.*, 2009). Nano scaled cobalt ferrites have attracted much more attention due to above mentioned characteristics in the field of biomedicine (S. C. Goha *et al.*, 2010), ferrofluid technology (V. K. Sankaranarayana *et al.*, 2003), advanced microelectronics (M. Suginoto *et al*, 1999) , high frequency data storage and microwave absorbing materials (G. Bate *et al*, 1991). Rare earth oxides are good electrical insulators with high electrical resistivity. In spinel ferrites the proper choice of rare earth cation can alter the electrical and magnetic properties and have a large influence upon the magnetic anisotropy of the system. Doping the parent spinel ferrite with rare earth

*Corresponding author. E-mail: Iftikhar_qau@yahoo.com, Tel: 0092-51-90855206

ions leads to structural disorder and lattice strain, thereby enhancing the electrical and magnetic parameters (S. E. Jacobo *et al.*, 2004; F. X. Cheng *et al.*, 1999) have studied the effect of rare earth ion substitution on Curie temperature. (B. R. Kumar *et al.*, 2002) have studied the thermoelectric properties of spinel ferrites doped with Gd^{3+}. (K. K. Bharathia *et al.*, 2009) have studied the magneto-electric properties of Gd^{3+} doped ferrites. (A. Rana *et al.*, 2011) have demonstrated the affect of Gd^{3+} substitution on dielectric properties of cobalt ferrite. Dielectric parameters of cubic spinel ferrites are important in understanding the electrical conduction, behavior of localized charge carrier's, and polarization phenomenon. Impedance spectroscopy is another important way to completely analyze all contributions to resistance in nano materials. According to different studies (D. Ravinder *et al.*, 2001; K. V. Kumar *et al.*, 2002) the concentration of rare earth doping in the ferrites is important while describing the electrical and magnetic properties of these ferrites. These unique characteristics of rare earth doped systems are due to 4fn electronic states (A. Maqsood *et al*., 2009).

In the present work we aimed to study the influence of a rare earth ion (Gd^{3+}) on structural, electrical and magnetic properties of Co-ferrites. We have successfully synthesized spinel type nano ferrites $CoGd_xFe_{2-x}O_4$ (x=0.0 to 0.1) by sol-gel auto combustion followed by heat treatment and characterization is done by XRD, FTIR, SEM, VSM, and LCR meter. We report a comprehensive study of structural, electrical (Dielectric, Impedance, AC conductivity) and magneto-crystalline anisotropy for gadolinium doped Co-ferrites in detail.

2. Experimental techniques

2.1. Synthesis

A nominal composition of $CoGd_xFe_{2-x}O_4$ with x ranging from 0.0 to 0.1 has been prepared by sol-gel auto combustion technique. All the chemicals purchased were of analytical grade and used as received. Aqueous solutions of Iron nitrate Fe $(NO_3)_3.9H_2O$, Gd $(NO_3)_3.6H_2O$ and Co $(NO_3)_2.6H_2O$ were prepared by dissolving stoichiometric amounts of nitrate salts in de-ionized water. Molar ratio of M^{3+} and M^{2+} were kept 2:1. Aqueous nitrates were then mixed with a magnetic stirrer. Aqueous solution of citric acid were prepared with the ratio of Nitrates/citric acid=1/1.5 and mixed with the nitrate solution. The mixed solution was magnetically stirred for 1 hr. The solution were then neutralized with aqueous ammonia and heated at 100^0C till the liquid turns to a gel. Gel then automatically converted to fluffy powders by self ignition. Prepared powders were then dried further in an electric oven at 100^0C for few hours. As synthesized material were then ground and palletized into disc shaped using a hydraulic press under a load of 6 tonns. Disc shaped pellets and powder were sintered at 600^0C for 4 hrs in a muffle furnace for further characterizations.

2.2. Characterization

The crystallographic information (Crystallite size, D *(311)*; lattice constant, (a); X-ray density, (D_x); and porosity (P), were found using indexed XRD patterns of the studied samples. XRD patterns were recorded using X-ray diffraction analysis (STOE-Seifert X'Pert PRO) at room temperature using CuKα (λ =1.5406 Å) radiation with 2-theta in the range of 20^0 to 80^0. The crystallite sizes were calculated and compared using the sherrer's formula and Williamson–Hall plots. W-H plots are usually drawn to see the strain effect in crystal structure. According to Williamson-Hall method (A. Ahlawat *et al.*, 2011) the width of individual reflections can be expressed as follows,

$$\beta cos\theta = k\lambda/D + 4\varepsilon sin\theta \quad (1)$$

where β is the width of peaks, D is the crystallite size, λ is the wavelength of Cu Kα radiation and ε is the crystal strain effect. The pellets of the samples were prepared using KBr for recording the FT-IR spectra in the range from 350 cm^{-1} to 1000 cm^{-1} at room temperature. The morphology and grain size was analyzed using SEM (JEOL-instrument JSM-6490A). The particle size patterns were recorded using atomic force microscopy (JEOL-JSPM-5200) at room temperature. A vibrating sample magnetometer was used to study the magnetic properties. DC electrical resistivity (ρ) was measured using two probe method at room temperature. Pellets (13mm in diameter) of samples were used for measuring the dielectric properties using precision impedance analyzer (Wayne Kerr 6500B) at room temperature. The real part of relative permittivity was calculated using the relation (R. C. Kamble *et al.*, 2010),

$$\varepsilon' = Cd/\varepsilon^0 A \quad (2)$$

where C is the capacitance of the pellet in farad, d the thickness of the pellet in meter, A the cross-sectional area of the flat surface of the pellet and ε^0 the constant of permittivity of free space. The dielectric tangent loss factor measured directly from the impedance analyzer. The dielectric loss (ε'') is also measured in terms of tangent loss factor (tanδ) and $\varepsilon^{/}$, defined by the following relation,

$$\varepsilon'' = tan\delta\ \varepsilon' \quad (3)$$

The AC conductivity can be calculated using the values of frequency and dielectric loss factors

$$\sigma_{AC} = 2\pi f \varepsilon^0 \varepsilon^{/} tan\delta \quad (4)$$

Complex impedance plane plots were drawn to study the electrical properties of $CoGd_xFe_{2-x}O_4$. The real ($Z^{/}$) and imaginary ($Z^{//}$) parts of impedance were calculated using the relations (K. M. Batoo *et al*, 2009),

$$Z^{/} = Z\ cos\theta \quad (5)$$

$$Z^{//} = Z\ sin\theta \quad (6)$$

where θ is the phase angle measured from impedance meter.

3. Results and Discussion

3.1. Structural Characterizations

The powder XRD patterns of Gd^{3+} doped Co-ferrites for

x=0.0 to x=0.1 have been presented in Fig.1. All the patterns can be easily indexed to cubic spinel crystal structure (Fd_3m) of $CoFe_2O_4$ (JCPDS card 22-1086) with (220), (311), (400), (511) and (440) diffraction peaks. Broad diffraction peaks represents the nanoscale crystallite size. It can be seen from the XRD patterns that crystallinity decreases by increase in the concentration of Gd^{3+} attributed to the decreased intensity in the observed peaks. Lattice parameter 'a' for all the samples has been calculated by interplanar spacing (d_{hkl}) and 2-theta values using the standard relation,

$a=d_{hkl}(h^2+k^2+l^2)^{1/2}$. Value of lattice constant for x=0.0 comes out to be 8.3865Å, well in agreement with reported value (Y. C. Mattei *et al.*, 2009). Lattice constant has increased monotonically with increment in Gd^{3+} concentration as shown in Table.1. This increase can be easily explained due to substitution of large ionic radii of Gd^{3+} (0.94Å) in place of smaller Fe^{3+} (0.67 Å) ions. Also rare earth ions are usually present at grain boundaries that cause hindrance in the grain growth, therefore crystal size and unit cell parameters increases. Peak broadening (FWHM) has been used to determine the crystallite sizes using the sherrer's formula. Average crystallite size calculated for most intense (311) peak comes out to be 16 nm to 25 nm ±2nm. It is observed that crystallite size also increased by increase in the Gd^{3+} concentration. This increase in lattice parameter and crystallite size induces a lattice strain in the crystal structure. This may be explained on the basis of defects present in the parent $CoFe_2O_4$, which allows the absorption of lattice strain caused by the higher dopant amounts (J. Peng *et al.*, 2011). The value of theoretical density has been calculated by the relation, $D_x=8M/Na^3$, where a^3 is unit cell volume. Theoretical density (D_x) and measured density (D_m) calculated from weight and dimensions both increases with increase in Gd^{3+} due to increase atomic weight of gadolinium ion. All the values of crystallite sizes, lattice constant and lattice strain have been presented in Table.1.

Fig.2 (a,b). Shows the W-H plots for x=0.0 and x=0.1 respectively. These plots have been drawn to measure the crystallite sizes and lattice strain and compared with the crystallite sizes calculated by sherrer's formula. The positive slopes of the Gaussian fit to the peak broadening shows a tensile strain present in the prepared samples that increases with increases in Gd^{3+} concentration owing to lattice distortion in the host crystal structure by Gd^{3+}. The behavior of the W-H plots also confirm the increase in crystallite size by doping of larger ion Gd^{3+} in Co-ferrites as more the positive slope larger is the crystallite size (A. Ahlawat *et al.*, 2011).

3.2. FT-IR Characterization

Fig.3 shows the FT-IR spectra for the studied sample at room temperature in a wave number range of 350 cm^{-1} to 1000 cm^{-1}. It can be observed that the entire spectrum in the described range shows to distinct peaks, one around 600 (υ_1) and the other near 375 (υ_2). The high frequency peak (υ_1) shows the metal oxygen vibration at tetrahedral sub-lattice (A-sites) and the low frequency peak (υ_2) attributes to the intrinsic vibrations of metal oxygen bond at octahedral sub-lattice (B-sites) (M. Shrivastava *et al.*, 2009). These two absorption bands are expected for the spinel structure of present ferrites synthesized by sol-gel auto combustion method. These vibrational bands for Gd^{3+} doped Co-ferrites are in a range of 559 cm^{-1} to 580 cm^{-1} for υ_1 and 370cm^{-1} to 381cm^{-1} for υ_2 as shown in Table.1. It has been observed that substitution of Gd^{3+} with Fe^{3+} causes shifts of band (Fe^{3+}–O^{2-}) towards higher frequency side due to increased bond length at B-sites and lattice distortion. This also suggests the occupancy of Gd^{3+} at B-sites for the present studied samples.

3.3. SEM Characterization

SEM images (fig.4) shows the surface morphology and grain size for the prepared sample x=0.0 and x=0.1. It is clear from the image that uniformly distributed; less agglomerated and homogenous spherical particles have been formed in a controlled environment by sol-gel auto combustion technique. Micrographs also confirm the increase in grain size with Gd^{3+} doping in the parent crystal structure. The homogeneity of shape and grain size largely affects the electrical and magnetic properties of ferrites.

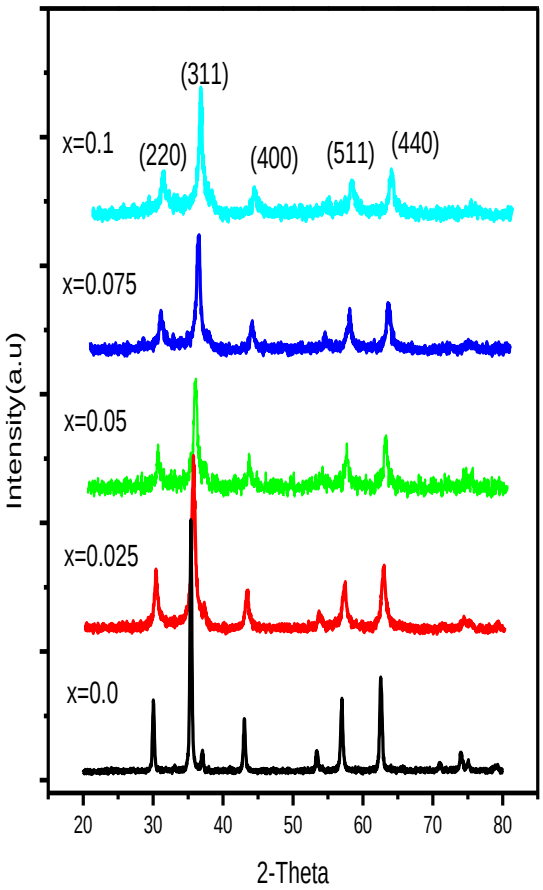

Figure.1 Indexed XRD patterns of $CoGd_xFe_{2-x}O_4$ (x=0.0 to x=0.1) nanoparticles synthesized by sol-gel auto combustion method

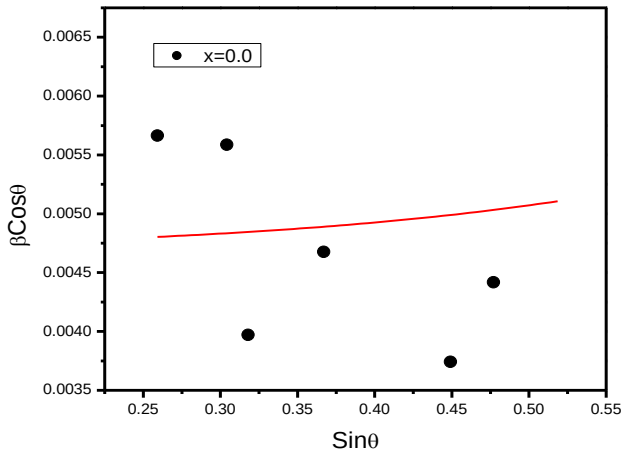

Figure.2 W-H plots for $CoGd_xFe_{2-x}O_4$ nanoparticles synthesized by sol-gel auto combustion method, (a) x=0.1 (b) x=0.0

3.4. AFM study

Atomic force microscopy is another excellent technique to study the morphology of the nano particles in the dispersed form. In support of the particle sizes observed from SEM, the particle sizes for the sample x=0.025 have been observed by AFM also as shown in the fig 5. It can be observed the well dispersed uniformly distributed and spherical morphology of the nano particles in the micrograph and the average particle sizes lies in the range of 23nm to 36 nm well in agreement with SEM data.

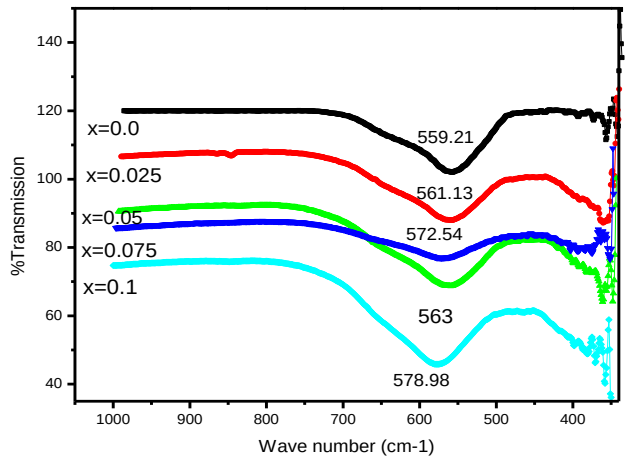

Figure.3 FTIR spectra for $CoGd_xFe_{2-x}O_4$ (x=0.0 to x=0.1) nanoparticles synthesized by sol-gel auto combustion method

3.5. Electrical Characterization

3.5.1. Variation of DC electrical resistivity

Fig.6 (a) shows the DC electrical resistivity of $CoGd_xFe_{2-x}O_4$ with composition (x=0.0 to x=0.1) of the dopant at room temperature. Co-ferrite is a highly resistive material with high activation energy. Method of synthesis, type and substitution of doped cations at A and B site, particle size and morphology and sintering temperatures largely affects the electrical properties of spinel ferrites (S. A. Mazen *et al.*, 2007). This can be observed from the graph that DC electrical resistivity decreases up to a concentration of x=0.025 but then increases with increase in Gd^{3+} concentration. There is a significant increase in the DC electrical resistivity with Gd^{3+} substitution (x=0.1). DC electrical resistivity was measured also in the temperature range of 368K to 573K fig.6 (b) using a Cu electrode and found a decrease in the resistivity due to increase in the temperature that confirms the semiconducting nature of Gd^{3+} doped cobalt ferrites. According to the Arrhenius relation,

$$\rho=\rho^0 e^{\Delta E/KBT} \quad (7)$$

Where ΔE is the activation energy measured from the slope of resistivity temperature plots, and K_B is the Boltzman constant. Resistivity decreases linearly with increase in temperature due to increase in the mobility of charge carriers by thermal agitation. Electrical conduction in spinel ferrites can be easily explained by Verwey mechanism (E. J. W. Verwey *et al.*, 1935) and is mainly due to electron hopping between Fe^{2+} and Fe^{3+}.

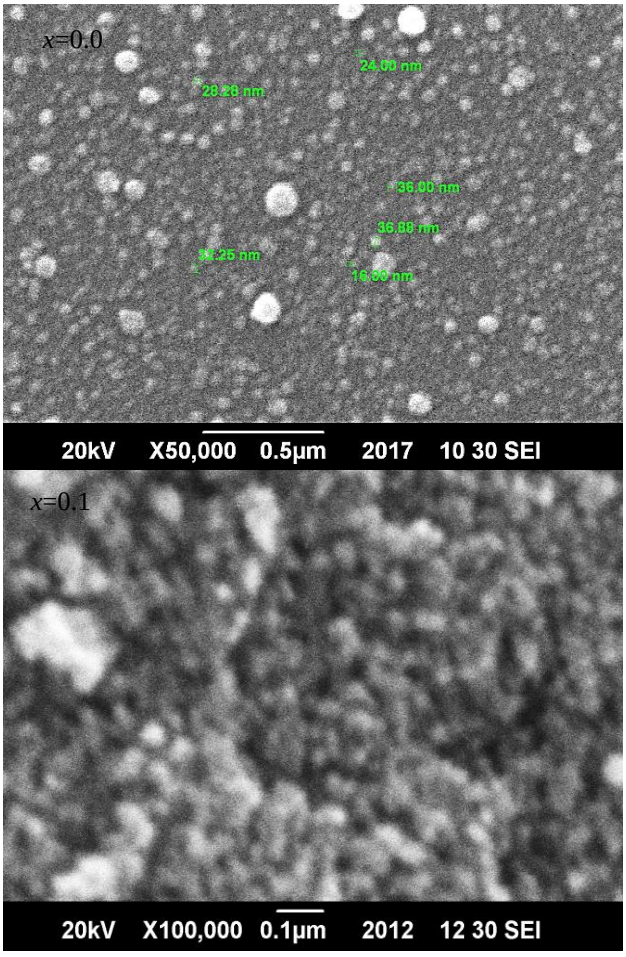

Figure.4 SEM images for $CoGd_xFe_{2-x}O_4$ (x=0.0) and (x=0.1) nanoparticles synthesized by sol-gel auto combustion method

The suggested cations distribution for the present samples of $CoGd_xFe_{2-x}O_4$ can be written as: $(Co^{2+}{}_{0.5}Fe^{3+}{}_{0.5})_A$

$(Co^{2+}_{0.5}Gd^{3+}_{x}Fe^{3+}_{1.5-x})_{B}O_4$. Gd^{3+} ion substitution in place of Fe^{3+} at octahedral (B site) decreases the number of Fe^{3+} ions at B sites which also decrease the hopping tendency between $Fe^{3+} \leftrightarrow Fe^{2+}$ ion pairs, thereby reducing the conductivity and increasing the DC electrical resistivity. The DC electrical resistivity variations with Gd^{3+} substitution can be explained as for x=0.025, Gd^{3+} ions occupy A site replacing Fe^{3+} due to which number of Fe^{3+} ions at B-site increases and thus Fe^{2+}. This may happen due to lattice distortion caused by doping a concentration of x=0.025. A low concentration of Gd^{3+} causes a severe change in centro-symmetric FCC structure of parent crystal that causes an increase in hopping of electron and a net electric polarization (M. Z. Said *et al.*, 1998). This reason is reflected in the high dielectric parameters and a sharp decrease in saturation magnetization for x=0.025.

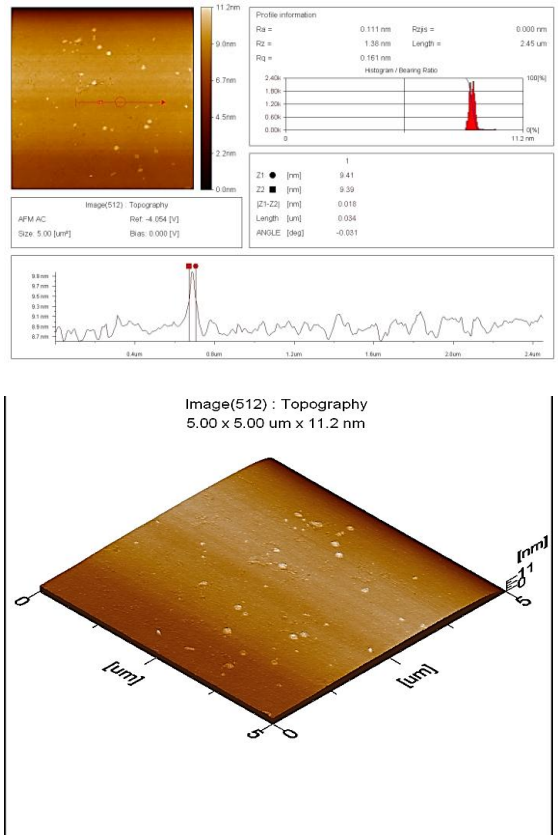

Fig.5 AFM micrograph for $CoGd_xFe_{2-x}O_4$ (x=0.025) nanoparticles synthesized by sol-gel auto combustion method

3.5.2. Dielectric study

As nanocrystalline spinel ferrites are good dielectric materials, depending upon the particle size, cation distribution and method of synthesis. Therefore different studies (M. A. Ahmed *et al*., 2003) and (F. Muthafar *et al*., 2011) have been provided relating the dielectric parameters of Gd^{3+} doped ferrites. Dielectric properties (real and imaginary parts of relative permittivity, dielectric loss tangent) for the prepared series of $CoGd_xFe_{2-x}O_4$ (x=0.0 to x=0.1) have been studied in the frequency range 1 kHz to 5MHz at room temperature. Figs7 and 8 show the real ($\varepsilon^{/}$) and imaginary ($\varepsilon^{//}$) part of relative permittivity with frequency at room temperature.

It can be observed from the figure that relative permittivity for all the samples decreases with increase in frequency and ultimately becomes constant at higher frequencies (~MHz). This decrease in permittivity is more rapid in the low frequency region but this decrease becomes sluggish as the applied frequency becomes higher. This behavior is subjected to dielectric polarization under the application of AC field. Permittivity and Resistivity both are electrical properties of ferrites and depends upon the conduction phenomenon. Hopping of electron between Fe^{2+} and Fe^{3+} is responsible for this conduction. This hopping is responsible for polarization at grain boundaries due to local charge displacement. Such kind of dielectric dispersion in ferrites can be explained by Maxwell-Wagner model (R. M. Mohamed *et al*., 2010) and koops theory (C. G. Koop's *et al*., 1951), which suggests that ferrite system consist of a combination of highly conducting grains separated by poorly conducting grain boundaries.

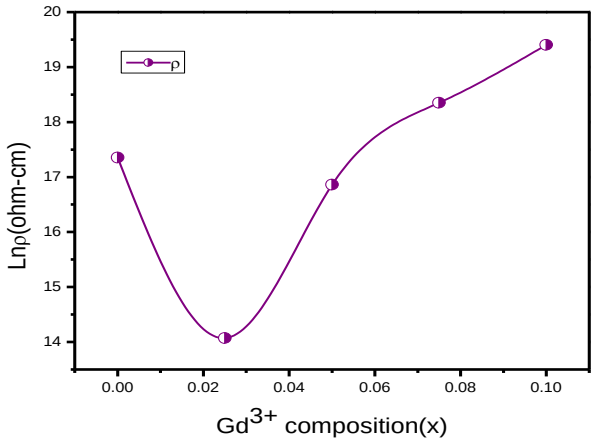

Figure.6 (a) Variation of DC electrical resistivity ($ln\ \rho$) with composition x (Gd^{3+}) for $CoGd_xFe_{2-x}O_4$ (x=0.0 to x=0.1) nanoparticles synthesized by sol-gel auto combustion method.

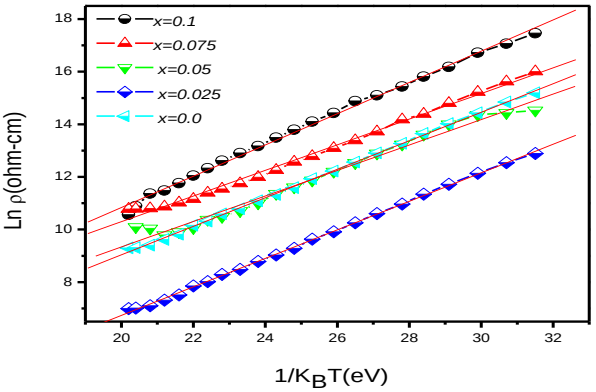

Figure.6 (b) Variation of DC electrical resistivity ($ln\ \rho$) with inverse of temperature $1/K_BT$ (eV) for $CoGd_xFe_{2-x}O_4$

(x=0.0 to x=0.1) nanoparticles synthesized by sol-gel auto combustion method

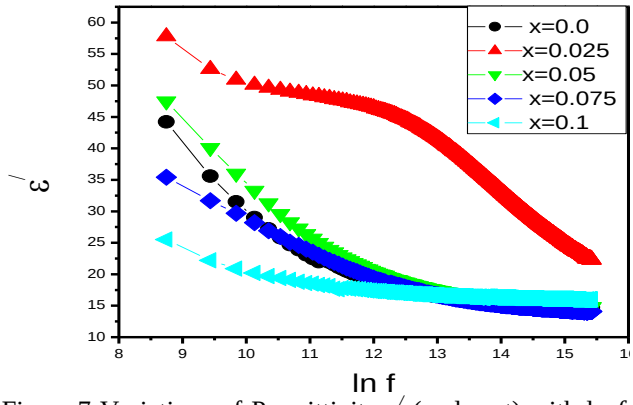

Figure.7 Variations of Permittivity $\varepsilon^{/}$ (real part) with ln f for $CoGd_xFe_{2-x}O_4$ (x=0.0 to x=0.1) nanoparticles synthesized by sol-gel auto combustion method

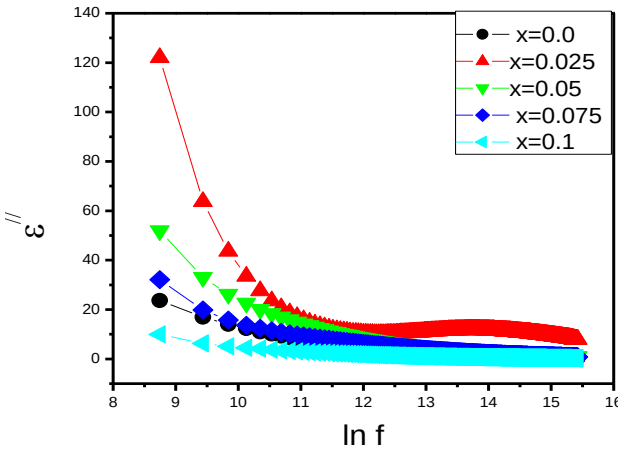

Figure.8 Variations of Permittivity $\varepsilon^{//}$ (imaginary part) with ln f for $CoGd_xFe_{2-x}O_4$ (x=0.0 to x=0.1) nanoparticles synthesized by sol-gel auto combustion method

Electrons by hopping pile up at grain boundaries due to high resistance and polarization takes place there. At high frequencies this hopping frequency does not follow up the field variation thereby making the relative permittivity a constant. Room temperature dielectric parameters have been presented in Table.1. It can be seen from the tabulated data that relative permittivity and losses increases with increase in Gd^{3+} concentration x=0.025 but after this concentration decreases to 12 for x=0.1. As dielectric polarization in ferrites is due to electron exchange $Fe^{2+} \leftrightarrow Fe^{3+}$, magnitude of which depends upon the percentage of Fe^{2+} and Fe^{3+} ion pairs at A and B sites. Fe^{2+} ions concentration largely affects the conduction phenomenon and depends upon type of cation substituting, synthesis route, sintering time and sintering temperatures. In the present case relative permittivity ($\varepsilon^{/}$ and $\varepsilon^{//}$) both increases for Gd^{3+} concentration x=0.025. Which can be explained by low Fe^{2+} ion concentration at B-site causing a low value of resistivity and hence a high value of dielectric parameter. As resistivity and relative permittivity has inverse behavior to each other (I. H. Gul *et al.*, 2008).

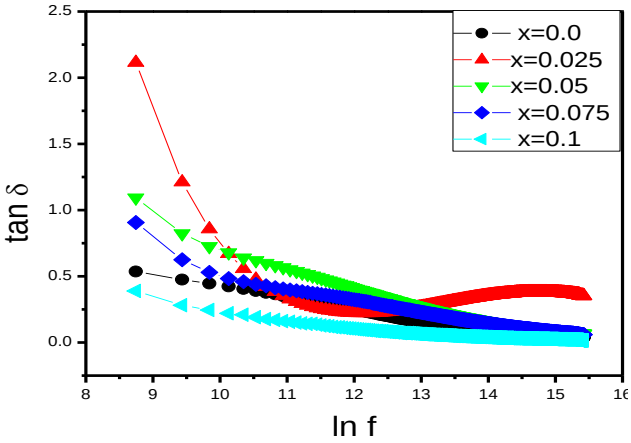

Figure.9 Variations of Dielectric loss tangent (*tanδ*) with ln f for $CoGd_xFe_{2-x}O_4$ (x=0.0 to x=0.1) nanoparticles synthesized by sol-gel auto combustion method

Fig.9 shows the variation of tanδ with frequency. It can be seen that dielectric loss tangent has the same trend as permittivity. It decreases with increase in frequency and becomes constant up to 5 MHz due to decreased polarization at high AC fields. This dielectric behavior reversed the trend that has been observed for DC-electrical resistivity. Dielectric losses in ferrite system usually reflect in DC electrical resistivity. Low loss dielectric material will be a highly resistive as well. Also observed that for x=0.025, a small peak is present owing to the relaxation phenomenon in ferrites (A. Verma *et al.*, 2011). Sample with x=0.1 shows a low loss dielectric behavior which allows its use in high frequency data reading/writing in electronic structures. Fig.10 shows the variation of AC conductivity for $CoGd_xFe_{2-x}O_4$ as a function of frequency (1 kHz-5MHz) for composition x=0.0 to x=0.1. It can be observed that AC conductivity increases linearly with frequency. This linear increase in AC conductivity relates with conduction by electron exchange between the ions of same element but difference valence states. As ferrites structure is cubic close pack lattice with cations at octahedral (B) site and tetrahedral (A) site. The exchange of electric charge between A-B sites is more important as compared to B-B exchange. On the application of AC field this electron exchange increases thereby increasing the AC conductivity (K. M. Batoo *et al.*, 2011). Usually AC conductivity can be represented as,

$$\sigma_{AC} = \sigma_0(T) + \sigma(\omega,T) \quad (8)$$

which is a combination of frequency independent term $\sigma_0(T)$ called as DC conductivity and frequency dependent term $\sigma(\omega,T)$ called as AC conductivity due to hopping of electrons at octahedral site. AC conductivity can be shown as,

$$\sigma_{AC} = A\omega^n \quad (9)$$

where A is term having units of conductivity and n is the slope of AC conductivity ($\ln\sigma_{AC}$) vs $\ln\omega$ plots Fig.10. Along with the increase in hopping phenomenon, the AC field promotes the formation of different charge carriers from different localized states. The charge centers help in increasing conductivity. According to (M. G. Chourashiya *et al.*, 2008), AC conductivity increases

linearly for structures consisting of grains and grain boundaries but for large polarons it decreases with increase in applied AC field.

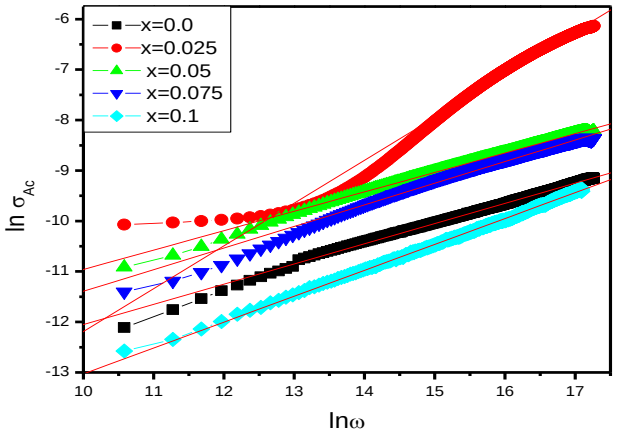

Figure.10 Variations of $ln\sigma_{AC}$ with $ln\omega$ for $CoGd_xFe_{2-x}O_4$ (x=0.0 to x=0.1) nanoparticles synthesized by sol-gel auto combustion method

3.5.3. Impedance study

Impedance analysis is useful to completely understand the electrical properties of spinel type ferrites and give us the data for both resistive (real part) and reactive (imaginary part) contribution to conductivity on the application of AC field (A. M. M. Farea *et al.*, 2008). Complex impedance plot also called as Nyquist diagrams gives a complete contribution of microstructure (grains and grains boundary) resistances. Fig.11 (a) and (b) shows the variations of real and imaginary parts of complex impedance with applied frequency (1 kHz to 5MHz). Both the resistance (Z') and reactance (Z'') decreases with increase in AC field showing the conduction is promoted by applied AC field. Fig.11 (c) shows the complex impedance plane plots (cole-cole) for all the studied samples. These complex plane plots help to distinguish the grain and grain boundary resistances and interfacial resistance of conducting electrodes. It is clear from the Nyquist plot that only one semi circle is present for all the studied samples in the low frequency region. As its shown in different studies (H. Ya *et al.*, 2008) and (W. Chen *et al.*, 2010) that there are two consecutive semi circles in complex impedance diagrams, one in low applied fields showing the grain boundary resistances and the other in high field side shows the grains contribution.

Only one quarter circle in low field region confirms the predominance of grain boundary resistance for the present studied samples of Gd^{3+} doped Co-ferrite and grain resistance is not well resolved. It can also be seen from complex plane plot that grain boundary resistance increases with increase in Gd^{3+} concentration for x=0.1.

3.6. Magnetic study

To study the effects of Gd^{3+} doping on magnetization, coercivity, remanent magnetization (*Mr*) and magneto-crystalline anisotropy (H_K) of Co-ferrite, M-H hysteresis loops were recorded using VSM under the applied magnetic field of 10 k Oe at room temperature. Fig.12 (a) shows the hysteresis curves for all the samples under investigation. It is clear that all the samples show a fine s shape loops with a decrease in magnetization (*Ms*) and

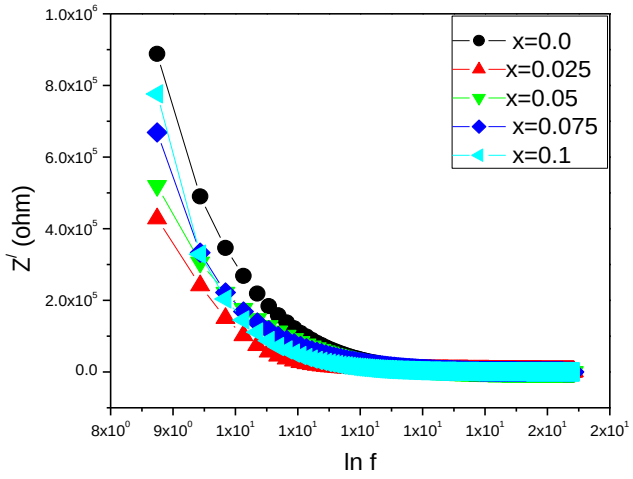

Figure.11 (a) Variations of Impedance Z' (real part) with ln f

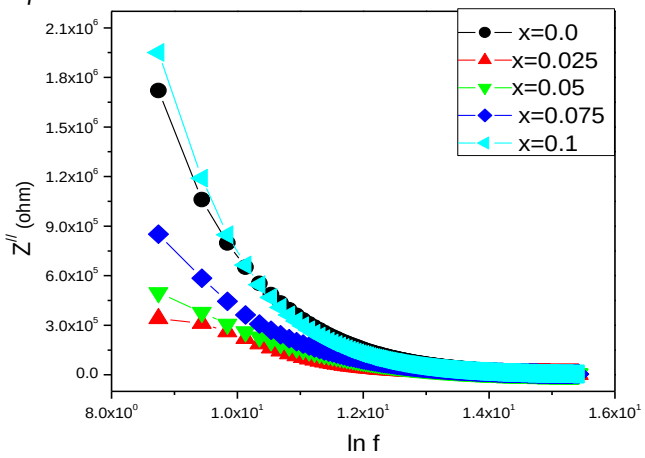

Figure.11 (b) Z'' (imaginary part) for $CoGd_xFe_{2-x}O_4$ (x=0.0 to x=0.1) nanoparticles synthesized by sol-gel auto combustion method

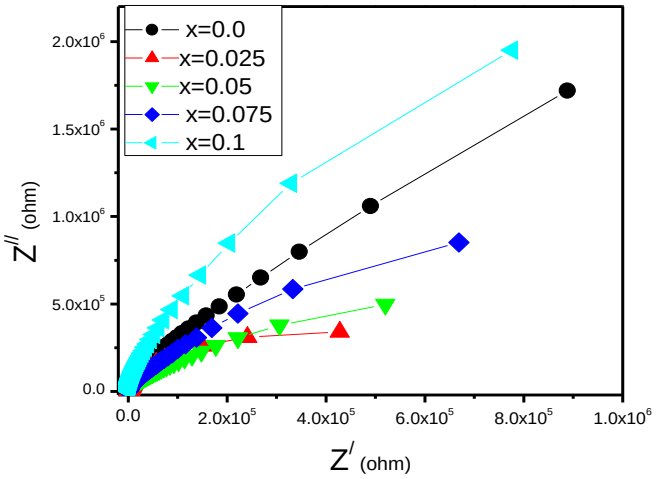

Figure.11 (**c**) Complex impedance plane plots for $CoGd_xFe_{2-x}O_4$ (x=0.0 to x=0.1) nanoparticles synthesized by sol-gel auto combustion method

coercivity (*Hc*) with increase in Gd^{3+} concentration. This is due to the substitution of Gd^{3+} in place of Fe^{3+} at B-sites. Gd^{3+} ions have a higher magnetic moment (7 μ_B) in place of Fe^{3+} that has 5 μ_B. The order in magnetic moments of rare earth ions is below room temperature (J. Peng *et al.*, 2011) due to this at room temperature Gd ion behaves as non magnetic that cause a decrease in saturation magnetization and coercivity. This substitution causes a lattice distortion that alters the magnetic characteristics of materials. Magnetic properties of ferrite materials largely based upon the grain size, cation substitution, and A-B exchange interactions (K. K. Bharathi *et al.*, 2009). Increase in the grain size and decrease of A-B super exchange interaction causes canting spins at the surface of nano particles that decreases the magnetic characteristics of the present samples as shown in fig.12 (b). Spin arrangement for the Co-Gd ferrites were analyzed by measuring the value of Bohr's magnetron by the relation,

$$n_B = (\sigma_s/5585) \times M_W \quad (10)$$

Using the calculated magnetic moment Yafet-Kittel (Y-K) angles was studied to see the spin arrangement in present ferrite system by the relation (K. Lawrence *et al.*, 2011),

$$n_B = (6+x)\, Cos\alpha_{Y\text{-}K} - 5(1-x) \quad (11)$$

where *x* represents the composition of doping ion. All the magnetic data including Y-K angles were presented in Table.2. Y-K angle increases with increase in Gd^{3+} concentration owing to triangular spin arrangement of ions and results in decreased A-B interactions (Y. Yafet *et al.*, 1952). In order to analyze the Gd^{3+} influence on magnetic anisotropy of Co-ferrites, value of anisotropy constant (K_1) is determined using Law of approach (LA) to saturation (fig.13). Cubic anisotropy constant (K_1) and anisotropy field (H_k) can be calculated by following equations (K. Maaz *et al.*, 2007),

$$H_k = 2K_1/\mu_0 M_s \quad (12)$$

$$K_1 = \mu_0 M_s (105b/8)^{1/2} \quad (13)$$

where μ_0 is the permeability of the free space, *Ms* is saturation magnetization from the fit, b is the parameter obtained from the fit. Data for anisotropy constant and anisotropy field (H_k) is mentioned in Table.2. Our results are in comparable to earlier reported values for Co-ferrites (L. Zhao *et al.*, 2006).

It is clear from the data that cubic anisotropy decreases with increase in gadolinium concentration. Pure cobalt ferrite is has high anisotropy constant and field due to occupation at B-sites. It decreases due to Gd^{3+} occupation at B-sites. Cubic anisotropy constant also decreased doping gadolinium showing a decrease in coercivity for present studied samples. The anisotropy parameters (anisotropy constant and field) are not decreasing monotonically but more abruptly due to differing concentration of doping ion. This behavior is showing a strong lattice distortion due to Gd^{3+} substitution.

Nano particles synthesized by sol-gel auto combustion method

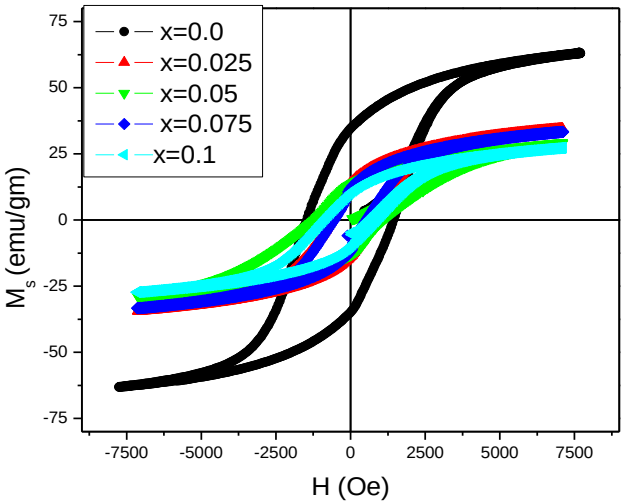

Figure.12 (a) *M-H* loops for $CoGd_xFe_{2-x}O_4$ (*x*=0.0 to *x*=0.1)

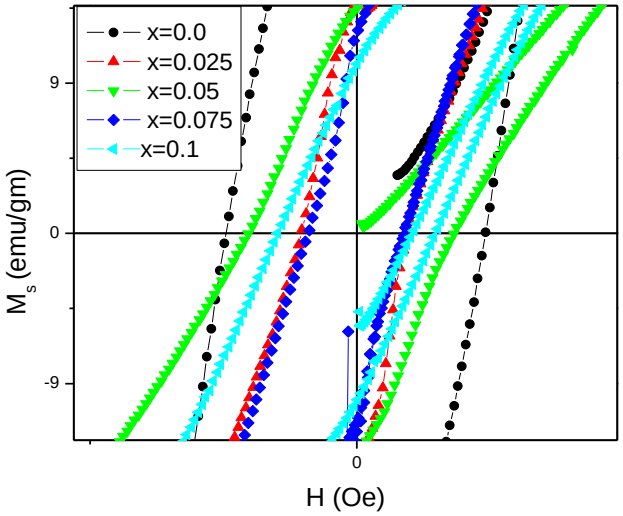

Figure.12 (b) Variation of Coercivity (*Hc)* with *x*=0.0 to *x*= 0.1

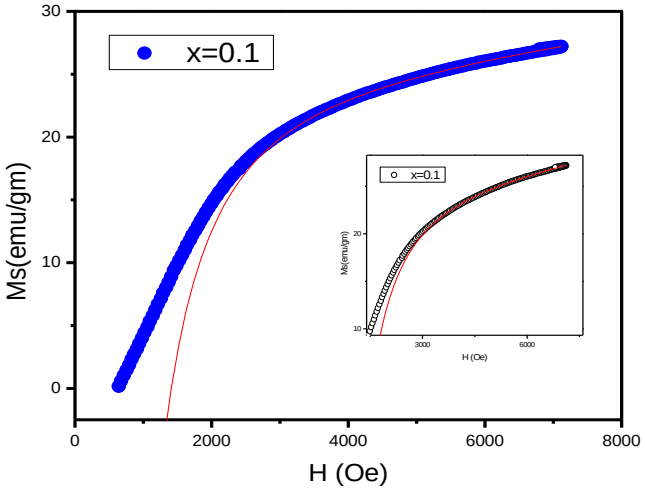

Figure.13 Fit to LA for $CoGd_xFe_{2-x}O_4$ (*x*=0.1) nanoparticles synthesized by sol-gel auto combustion method

Table.1 Crystallite size (D_{311}) Sherrer's method, Crystallite size D (W-H) method, lattice parameter (a) , X-ray density (D_x), measured density (D_m), Porosity (P), FTIR vibrational Waver numbers (υ_1 and υ_2) , Dielectric constant (ε'), Dielectric loss factor (ε''), and tangent loss ($tan\delta$), AC conductivity (σ_{AC}), n (conductivity parameter)

Composition	***x=0.0***	***x=0.025***	***x=0.05***	***x=0.075***	***x=0.1***
Lattice constant 'a' (Å)	8.3865	8.3874	8.3947	8.3954	8.4162
D(311) nm	16.92	16.99	21.75	21.93	22.54
$D_m\,(gm/cm^3)$	2.47	2.48	2.511	2.523	2.57
$D_x(gm/cm^3)$	5.29	5.35	5.38	5.41	5.45
P (%)	53.3	53.6	53.3	53.4	52.8
$\upsilon_1(cm^{-1})$	559.21	561.13	563	572.54	578.98
$\upsilon_2(cm^{-1})$	370.35	370.87	377.9	378.3	380.76
ρ (Ω-cm)	$3.45x10^7$	$1.29x10^6$	$2.10x10^7$	$9.31x10^7$	$2.67x10^8$
ε' *(1MHz)*	15.2	34.9	16.1	15.1	13.6
ε''*(1MHz)*	1.19	11.9	2.81	2.41	0.4
tanδ(1MHz)	0.077	0.3463	0.1750	0.1568	0.043772
ε'*(5 MHz)*	14.2	22.3	14.8	14.1	12
ε''*(5 MHz)*	0.473	7.86	0.97	0.842	0.156
tanδ(5 MHz)	0.0324	0.3520	0.0654	0.0598	0.0160
σ_{AC}*(5 MHz)*	$1.31x10^{-4}$	$2.17x10^{-3}$	$2.34x10^{-4}$	$2.7x10^{-4}$	$7.14x10^{-5}$
n	0.4	0.85	0.39	0.42	0.51

Table.2 Saturation magnetization (Ms), Remanance (Mr), Coercivity (Hc), Remanance ratio (Mr/Ms), Magnetic moments (n_B), Yeffit-Kittel angle ($\alpha_{y\text{-}k}$), Magnetic anisotropy constants (K_1), Anisotropy field (H_k)

Composition	***x=0.0***	***x=0.025***	***x=0.05***	***x=0.075***	***x=0.1***
M_s	63	34.5	28.73	33.32	27.26
H_c	2929	1096	2308	1078	1779
M_r	34.52	14.03	13.49	11.99	10.03
M_r/M_s	0.55	0.40	0.47	0.36	0.37
n_B	1.017	0.59	0.49	0.57	0.46
$\alpha_{Y\text{-}K}$	0	24.74	29.97	31.17	35.52
$K_1(erg/cm^3)$	$0.35x10^6$	$0.1x10^6$	$0.13\ x10^6$	$0.108\ x10^6$	$0.12\ x10^6$
$H_k(KOe)$	11.55	7.245	12.96	8.067	10.424

4. Conclusions

In summary nano sized $CoGd_xFe_{2-x}O_4$ with *x* ranging from 0.0 to 0.1 has been synthesized by sol-gel auto combustion. All the studied samples are pure cubic spinel type ferrites without any impurity phase. Lattice constant and crystallite size increases with increase in Gd^{3+} concentration, owing to increased ionic radii and atomic weight of gadolinium as compared to Fe^{3+}. Substitution of Gd^{3+} ion in parent crystal causes a lattice distortion that can be observed by increased lattice strain in W-H plots. DC electrical resistivity increases significantly to $2.67x10^8$ with Gd^{3+} substitution except for x=0.025 (~ 10^6). Dielectric properties (real and imaginary relative permittivity and dielectric loss tangent), decreases with increase in the dopant concentration showing that the material with x=0.1 is a low loss dielectric. AC conductivity increases with increase in Gd^{3+} composition showing a lattice disorder due to replacing Fe^{3+} by Gd^{3+} ion. Also a linear rise in conductivity with applied field indicates small polarons conduction mechanism. Impedance study reveals that the grain boundary are offering more resistance to conduction showing that smaller grains with more grain boundaries are formed for present samples. Gd^{3+} substitution have tailored the magnetic properties of Co-ferrites due to influence on A-B exchange of electrons. Saturation magnetization, coercivity and remanance all decreases with increase in dopant concentration. Yeffit-Kittel angles increases with *x*, showing a triangular spin arrangement for present ferrite system. Magnetic anisotropy of Co-ferrites decreases with increase in Gd^{3+} concentration (*x*). Thus the rare earth (Gd^{3+}) doped Co-ferrites found an application as high resistivity and low loss dielectric material in radio and microwave frequency applications.

Acknowledgment

The authors would like to acknowledge TWAS, Italy, Higher Education Commission (HEC) Islamabad Pakistan project No.1326, for providing financial support for this work and Pakistan science foundation (PSF) project.No.147.

References

R. Valenzuela (2012), Novel application of soft ferrites, *Phys. Res. Inter*, Vol. 2012 , pp.1-9

L. B. Tahar, M. Artus, S. Ammar, L.S. Smiri, F. Herbst, M. J. Vaulay, V. Richard, J. M. Grene`che, F. Villain, F. Fievet (2008), Magnetic properties of $CoFe_{1.9}RE_{0.1}O_4$ nanoparticles (RE) prepared in polyol, *J. Magn. Magn. Mater*, Vol. 320, pp.3242-3250.

M. A. Elkestawy, S. A. Kader, M. A. Amer (2010), AC conductivity and dielectric properties of Ti-doped $CoCr_{1.2}Fe_{0.8}O_4$ spinel ferrite, *Physica. B*, Vol. 405, pp.619-624.

Y. I. Kim, D. Kim, C. S. Lee (2003), Synthesis and characterization of $CoFe_2O_4$ magnetic nanoparticles prepared by temperature-controlled coprecipitation method, *Physica. B*, Vol. 337, pp.42–50.

C. S. Kim, Y. S. Yi, K. T. Park, H. Namgung, J. G. Lee (1999), Chemically prepared magnetic nanoparticles, *J. Appl. Phys*, Vol. 85, pp.5223–5225.

J. Peng, M. Hojamberdiev, Y. Xu, B. Cao, J. Wang, H. Wu (2011), Hydrothermal synthesis and magnetic properties of gadolinium doped $CoFe_2O_4$ nanoparticles, *J. Magn. Magn. Mater*, Vol. 323, pp.133-138.

V. Pillai, D. O. Shah (1996), Synthesis of high-coercivity cobalt ferrite particles using water-in-oil microemulsions, *J. Magn. Magn. Mater*, Vol. 163, pp.243–248.

W. Cai, J. Q. Wan (2007), Facile synthesis of superparamagnetic magnetite nanoparticles in liquid polyols, *J. Colloid. Interface. Sci*, Vol. 305, pp.366–370.

E. E. Sileo, S. E. Jacobo (2004), Gadolinium-Nickel ferrites prepared from metal citrates precursors, *Physica. B*, Vol. 354, pp.241-245

M. M. Rashad, R. M. Mohamed, H. El-Shall (2008), Magnetic properties of nanocrystalline Sm substituted $CoFe_2O_4$ synthesized by citrate precursor method, *J. Mater. Proc. Technol*, Vol. 198, pp.139–146.

K. S. Rao, A. M. Kumara, M. C. Varmaa, R. K. Choudary, K. H. Rao (2009), Cation dirtibution of Ti doped cobalt ferrites, *J. Alloys. Compd*, Vol. 488, pp.6–9

S. C. Goha, C. H. Chiaa, S. Zakariaa, M. Yusoffa, C. Y. Hawa, Sh. Ahmadia, N. M. Huangb, H. N. Lim (2010), Hydrothermal preparation of high saturation magnetization and coercivity cobalt ferrite nano crystals without subsequent calcinations, *J. Mater. Chem. Phys*, Vol.120, pp.31–35.

V. K. Sankaranarayana, C. J. Sreekumar (2003), A strategic approach for preparation of oxide nanomaterials, *J. Curr. Appl. Phys*,Vol. 3, pp.205–208.

M. Suginoto (1999), The past present and future of ferrites, *J. Am. Ceram. Soc*, Vol. 82, pp.269-280.

G. Bate, Magnetic recording materials since 1975, *J. Magn. Magn. Mater*, Vol. 100, pp.413-424.

S. E. Jacobo, S. D. Uhalde, H. R. Bertorello (2004), Rare Earth influence on the structural and magnetic properties of NiZn ferrites, *J. Magn. Magn. Mater*, Vol. 272, pp.2253-2254.

F. X. Cheng, J. T. Jia, Z. G. Xu, B. Zhou, C. S. Liao, C. H. Yan, L. Y. Chen, H. B. Zhao (1999), Microstructure, magnetic, and magneto-optical properties of chemical synthesized Co-RE (RE=Ho, Er, Tm, Yb, Lu) ferrite nanocrystalline films, *J. Appl. Phys*. Vol. 86, pp.2727–2732.

B. R. Kumar, D. Ravinder (2002), Electrical Conductivity of Ni-Zn-Gd Ferrites, *Mater. Lett*, Vol. 53, pp.441-445.

K. K. Bharathi, J. A. Chelvane, G. Markandeyulu (2009), Magnetoelectric properties of Gd and Nd-doped nickel ferrite, *J. Magn. Magn. Mater*, Vol. 32, pp.3677-3680.

A. Rana, O. P. Thakur, V. Kumar (2011), Effect of Gd^{3+} substitution on dielectric properties of nano cobalt ferrite, *Mater. Lett*, Vol. 65, pp.3191–3192.

D. Ravinder, K. V. Kumar, P. Balaya (2001), High-frequency dielectric behavior of gadolinium substituted Ni–Zn ferrites, *Mater. Lett*, Vol. 48, pp.210–214.

K. V. Kumar, D. Ravinder (2002), Electrical conductivity of Ni–Zn–Gd ferrites, *Mater. Lett*, Vol. 52, pp.166–168.

A. Maqsood (2009), Phase transformations in Ho2Si2O7 ceramics, *J. Alloys. Compd*, Vol. 471, pp.432-434.

A. Ahlawat. et al (2011), *J. Magn. Magn. Mater*, Vol. 323, pp.2049-2054.

R. C. Kamble, N. R. Adhate, B. K. Chougule, Y. D. Kolekar (2010), Magnetic and dielectric properties of mixed spinel Ni-Zn ferrites synthesized by citrate precursor method, *J. Alloys. Compd*, Vol. 491, pp.372-377.

K. M. Batoo, S. Kumar,C. G. Lee, Alimuddin (2009), Study of ac impedance spectroscopy of Al doped MnFe2−2*x*Al2*x*O4, *J. Alloys. Compd*, Vol. 480, pp.596-604.

Y. Ceden˜o-Mattei, O. Perales-Pe´rez (2009), Synthesis of high-coercivity cobalt ferrite nanocrystals, *J. Microelectronics*, Vol. 40, pp.673-681.

M. Srivastavaa, A. K. Ojhaa, S. Chaubey, A. Materny (2009), Synthesis and optical characterization of nanocrystalline $NiFe_2O_4$ structures, *J. Alloys. Compd*, Vol. 481, pp.515-519.

S. A. Mazen, H. M. Zaki, S. F. Mansour (2007), The infrared absorption and dielectric properties of Li–Ga ferrite, *Int, J. pure. Appl. Phys*, Vol. 3.No.1, pp.40-46.

E. J. W. Verwey (1935), Verway transitions in magnetite, *Ziest. F. Krist*, Vol. 91, pp.65.

M. Z. Said (1998), Effect of gadolinium substitution on the structural and electrical conductivity of Ni-ferrite, *Mater. Lett*, Vol. 34, pp.305-307.

M. A. Ahmed, E. Ateia, S. I. El-Dek (2003), Rare earth doping effect on the structural and electrical properties of Mg–Ti ferrite, *Mater. Lett*, Vol. 57, pp.4256–4266.

F. Muthafar, Al–Hilli, Li. Sean, S. Kassim (2011), Gadolinium substitution and sintering temperature dependent electronic properties of Li–Ni ferrite, *J. Mater. Chem. Phys*, Vol. 128, pp.127–132.

R. M. Mohamed, M. M. Rashad, F. A. Haraz , W. Sigmund (2010), Structure and magnetic properties of nanocrystalline cobalt ferrite powders synthesized using organic acid precursor method, *J .Magn. Magn. Mater*, Vol. 322, pp.2058-2064.

C. Koop's (1951), On the dispersion of resistivity and dielectric constant of some semiconductors at audio frequencies**,** *Phys. Rev*, Vol. 83, pp.121-126.

I. H. Gul, A. Maqsood (2008), Structural, magnetic and electrical properties of cobalt ferrites prepared by the sol–gel route, *J. Alloys. Compd*, Vol. 465, pp.227-231.

A. Verma, O. P. Thakur, J. H. Hsu (2011), Temperature dependence of electrical properties of nickel-zinc ferrites processed by the citrate precursor technique, *J. Alloys. Compd*, Vol. 509, pp.5315-5321.

K. M. Batto (2011), Study of dielectric and impedance properties of Mn ferrites, *Physica. B*, Vol. 406, pp.382-391.

M. G. Chourashiya, J. Y. Patil, S. H. Pawar, L. D. Jadhav (2008), Studies on the structural, morphological and electrical properties of Ce_{1-x} Gd_x $O_{2-(x/2)}$, *J. Mater. Chem. Phys*, Vol. 109, pp.39-44.

A. M. M. Farea, S. Kumar, K. M. Batoo, A. Yousef, C.G. Lee, Alimuddin (2008), Structure and electrical properties of $Co_{0.5}Cd_xFe_{2.5-x}O_4$ ferrites, *J. Alloys. Compd*, Vol. 464, pp.361–369.

H. Ya, R. B. Jackman, P. Hing (2008), Spectroscopic impedance study of nanocrystalline diamond films, *J. Appl. Phys*, Vol. 94, pp.7878-7883.

W. Chen, W. Zhu, C. Ke, Z. Yang, L. Wang, X. F. Chen, O. K. Tan (2010), Impedance spectroscopy and conductivity mechanism of CoFe(2)O(4)-Pb(Zr(0.53)Ti(0.47))O(3) composite thick films, *J. Alloys. Compd*, Vol. 508, pp.141-146.

Y. Yafet, C. Kittel (1952), Antiferromagnetic Arrangements in Ferrites, *Phys. Rev*, Vol. 87, pp.290-294.

K. Maaz, A. Mumtaz, S. K. Hasanain, A. Ceylan (2007), Synthesis and magnetic properties of cobalt ferrite ($CoFe_2O_4$) nanoparticles prepared by wet chemical route, *J. Magn. Magn. Mater*, Vol. 308, pp.289-296.

L. Zhao, H. Yang, L. Yu, Y. Cui, X. Zhao, S. Feng (2006), Study on magnetic properties of nanocrystalline La-, Nd-, orGd-substituted Ni–Mn ferrite at low temperatures, *J. Magn. Magn. Mater* , Vol. 305, pp.91-94.

K. Lawrence, K. Manoranjan (2011), Influence of Al^{3+}ion concentration on the crystal structure and magnetic anisotropy of nanocrystalline spinel cobalt ferrite, *J. Magn. Magn. Mater*, Vol. 323, pp.2042-2048.